



Activation of amorphous Bi_2WO_6 with synchronous Bi metal and Bi_2O_3 coupling: Photocatalysis mechanism and reaction pathway

Wenjie He^a, Yanjun Sun^a, Guangming Jiang^{a,*}, Hongwei Huang^b, Xianming Zhang^a, Fan Dong^{a,c,**}



^a Chongqing Key Laboratory of Catalysis and New Environmental Materials, College of Environment and Resources, Engineering Research Center for Waste Oil Recovery Technology and Equipment of Ministry of Education, Chongqing Technology and Business University, Chongqing 400067, China

^b Beijing Key Laboratory of Materials Utilization of Nonmetallic Minerals and Solid Wastes, National Laboratory of Mineral Materials, School of Materials Science and Technology, China University of Geosciences, Beijing 100083, China

^c The Center of New Energy Materials and Technology, School of Materials Science and Engineering, Southwest Petroleum University, Chengdu 610500, China

ARTICLE INFO

Keywords:

Amorphous Bi_2WO_6
Bi metal
Surface plasmon resonance
In situ FT-IR
Reaction mechanism

ABSTRACT

Amorphous semiconductors usually suffer from low photocatalysis efficiency due to the fast charge recombination rate. In this work, to activate the amorphous Bi_2WO_6 , Bi_2O_3 and Bi particles were in sequence deposited over its surface via a facile in situ chemical reduction of amorphous Bi_2WO_6 by NaBH_4 at room temperature. In the resultant ternary $\text{Bi}/\text{Bi}_2\text{O}_3/\text{Bi}_2\text{WO}_6$, the well-formed heterojunctions (i.e. $\text{Bi}-\text{Bi}_2\text{O}_3$ and $\text{Bi}_2\text{O}_3-\text{Bi}_2\text{WO}_6$) and the surface plasmon resonance effect of Bi both contribute to an increase in charge carrier concentration, an efficient e^-/h^+ separation and then an enhanced visible light photocatalytic performance. The molar ratio of Bi, Bi_2O_3 and Bi_2WO_6 in composite can be modulated by the dosage of NaBH_4 , and consequently the amount of each heterojunction (i.e. $\text{Bi}/\text{Bi}_2\text{O}_3$ or $\text{Bi}_2\text{O}_3/\text{Bi}_2\text{WO}_6$) as well as the intensity of SPR effect could be tuned. The photocatalytic NO removal test under visible light irradiation shows that BWO-0.8 (0.8 denotes the molar ratio of NaBH_4 to Bi_2WO_6) presents a maximum NO removal efficiency of 55.4%, much higher than that of the pristine amorphous Bi_2WO_6 (10%). The enhanced activity can be attributed to the balanced SPR effect of Bi metal and the heterojunction effect, making their overall contribution maximized. The pathway study of photocatalytic NO oxidation by in situ FT-IR suggests that NO is converted to nitrates adsorbed over the catalyst surface. The present work could provide a new approach to activate the amorphous semiconductors for efficient visible light photocatalysis.

1. Introduction

Environmental pollution and energy shortage are the two major challenges faced by human beings. Photocatalytic technology [1] is considered to be the most promising solution, which is featured by the direct utilization of solar energy to produce chemical fuels [2–4] and mineralize environmental pollutants [5–11]. Photocatalyst is the key part in this technology, and till now, numerous efforts have been devoted to the design and synthesis of robust catalysts with intense absorption/utilization of the solar light in broad spectra, a high electron/hole separation efficiency, and a suitable band energy for redox reactions [12,13]. Bi_2WO_6 is one typical semiconductor photocatalyst with an appealing layer structure composed of alternating bismuth oxide $(\text{BiO})^+$ and octahedral $(\text{WO}_4)^{2-}$ [14]. Furthermore, it has a visible-

light-response gap of 2.8 eV with the conducting and valence band edge lying at 0.46 and 3.26 eV, respectively. The more positive valence band over the redox potential of $\text{OH}^-/\cdot\text{OH}$ (1.99 eV) enables the Bi_2WO_6 to yield very oxidative $\cdot\text{OH}$ for pollutant degradation [15–18].

Room temperature method usually leads to the formation of amorphous Bi_2WO_6 [19–24], which is, however, inert in photocatalysis. The amorphous structure-induced deactivation usually originates from the abundant bulk defects in the disordered crystal, which work as the charge recombination centers [25]. To activate the amorphous Bi_2WO_6 , one well-defined solution is to reduce the number of the bulk defects by enhancing the particle crystallinity [26–29]. Amano et al. [30] employed a high-temperature hydrothermal treatment to improve the crystalline of Bi_2WO_6 and consequently acquired a highly enhanced photocatalytic activity. Another efficient strategy is to introduce one

* Corresponding author.

** Corresponding author at: Chongqing Key Laboratory of Catalysis and New Environmental Materials, College of Environment and Resources, Engineering Research Center for Waste Oil Recovery Technology and Equipment of Ministry of Education, Chongqing Technology and Business University, Chongqing 400067, China.

E-mail addresses: jiangguangming@zju.edu.cn (G. Jiang), dfctbu@126.com (F. Dong).

more cocatalyst on the surface. Very recently, Li succeeded to activate the amorphous Bi_2O_3 by depositing Bi NPs over its surface [31]. It is demonstrated that the activation results from (i) the construction of the Bi/ Bi_2O_3 heterojunctions and (ii) the SPR effect of Bi NPs. As we know, plasmonic metal Bi NPs is capable of concentrating incident photon energy into plasmon oscillations, which can be converted to a local electromagnetic field to promote the e^-/h^+ separation [32]. Till now, the metallic Bi with SPR effect have been extensively coupled with various photocatalysts, such as BiOCl [33], Bi_2MoO_6 [34], $g\text{-C}_3\text{N}_4$ [35,36], and reinforced their photocatalytic performance [37]. However, the activation of amorphous Bi_2WO_6 with Bi metal has never been reported.

In this work, Bi_2O_3 and Bi metal were in sequence deposited on the amorphous Bi_2WO_6 via a facile *in situ* reduction of Bi_2WO_6 by NaBH_4 at room temperature. The relative ratio of Bi, Bi_2O_3 and Bi_2WO_6 can be finely tuned by the dosage of NaBH_4 . The photocatalytic performance of this ternary composite was evaluated by photocatalytic removal of ppb-level NO under visible light irradiation. The phase structure, microstructure and optical property of the as-prepared catalysts were characterized. As an exciting result, the Bi/ Bi_2O_3 / Bi_2WO_6 exhibited a highly enhanced photocatalytic activity in comparison to the initial amorphous Bi_2WO_6 . In addition, a photocatalytic NO oxidation mechanism on Bi/ Bi_2O_3 / Bi_2WO_6 was proposed based on the observation of the reaction intermediates by *in situ* FT-IR. The present work could provide new strategy to activate the abundant amorphous semiconductors for highly efficient visible light photocatalytic air purification.

2. Experimental

2.1. Catalyst preparation

All the chemicals are of analytical grade and used without further purification. The Bi/ Bi_2O_3 /amorphous Bi_2WO_6 composites were prepared by a facile *in situ* wet-chemical reduction method with pure amorphous Bi_2WO_6 as the substrate. The amorphous Bi_2WO_6 was obtained by a traditional hydrothermal method: 1.390 g $\text{Bi}(\text{NO}_3)_3 \cdot 5\text{H}_2\text{O}$ was added to 40 mL deionized water, and dispersed by ultra-sonication and magnetic stirring for 10 min, forming a homogenous white suspension. Then, 0.473 g of $\text{Na}_2\text{WO}_4 \cdot 2\text{H}_2\text{O}$ pre-dissolved in 20 mL water was dropwise added, and the mixture was stirred for 1 h at room temperature. After that, the resultant white suspension was transferred into a 100 mL Teflon-lined stainless autoclave and kept reaction at 100 °C for 20 h. After cooling, the product was washed repeatedly by deionized water and ethanol, and then dried at 60 °C for 12 h.

Bi/ Bi_2O_3 / Bi_2WO_6 samples were then synthesized by using the above amorphous Bi_2WO_6 as the precursor and NaBH_4 solution as the reducing agent. By controlling the ratio of NaBH_4 to Bi_2WO_6 , series of Bi/ Bi_2O_3 / Bi_2WO_6 with different contents of Bi and Bi_2O_3 could be obtained. In detail, 1.5 g of pure amorphous Bi_2WO_6 powders were added into 20 mL deionized water with a further continuous stirring for 30 min. Then, 20 mL of NaBH_4 solution with different NaBH_4 / Bi_2WO_6 molar ratios of 0.2, 0.5, 0.8, 1.0, and 1.2 was dropwise added into the amorphous Bi_2WO_6 suspensions, respectively. After reaction for 30 min, the products were collected and washed with deionized water and absolute ethanol or twice and dried at 40 °C for 12 h in a drying oven. According to the NaBH_4 / Bi_2WO_6 molar ratios, the products were denoted as BWO-0.2, BWO-0.5, BWO-0.8, BWO-1.0 and BWO-1.2, respectively.

2.2. Characterization

The crystal phase of Bi_2WO_6 was analyzed by X-ray diffraction (XRD) with $\text{Cu K}\alpha$ radiation (model D/max RA, Rigaku Co., Japan). X-ray photoelectron spectroscopy (XPS) with $\text{Al K}\alpha$ X-rays ($\hbar\nu = 1486.6$ eV) radiation operated at 150 W (Thermo ESCALAB 250, USA) was used to investigate the surface properties. Scanning electron

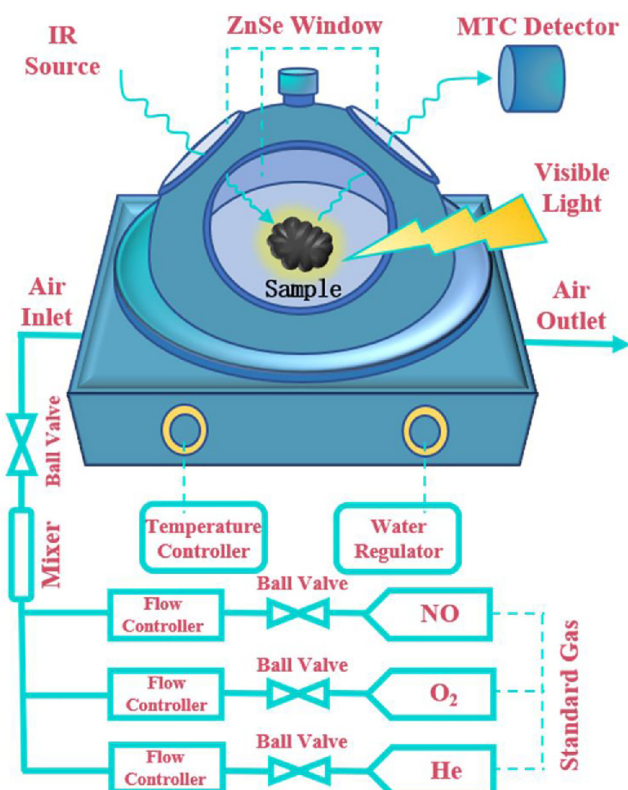


Fig. 1. Scheme of the *in situ* FT-IR analysis cell equipped with visible light illumination.

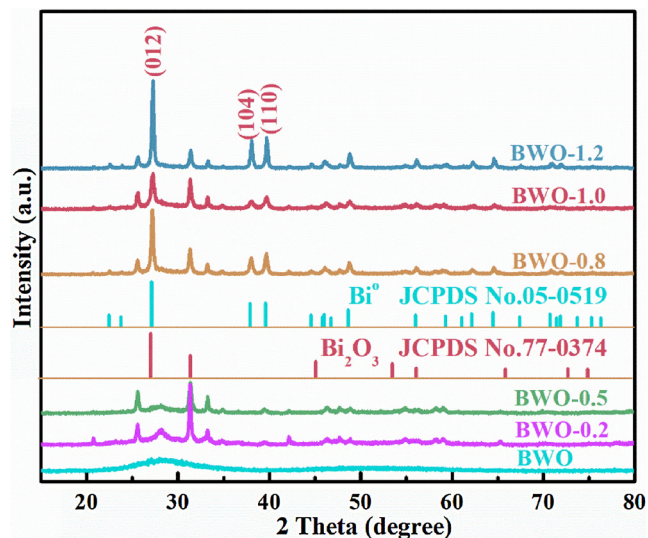


Fig. 2. The XRD pattern of pure Bi_2WO_6 and BWO-X ($X = 0.2, 0.5, 0.8, 1.0$ and 1.2).

microscopy (SEM, model JSM-6490, JEOL, Japan) and transmission electron microscopy (TEM, JEM-2010, JEOL, Japan) were used to characterize the morphology and structure of Bi_2WO_6 . N_2 adsorption-desorption isotherms were obtained on N_2 adsorption apparatus (ASAP 2020, Micromeritics, USA). The UV-vis diffuse-reflectance spectrometry (UV-vis DRS) spectrum was obtained for the dry-pressed disk samples using a scanning UV-vis spectrophotometer (UV2550, Shimadzu, Japan) equipped with an integrating sphere assembly, using 100% BaSO_4 as the reflectance sample. Steady and time-resolved fluorescence emission spectra were recorded at room temperature with a fluorescence spectrophotometer (Edinburgh Instruments, FLSP-920).

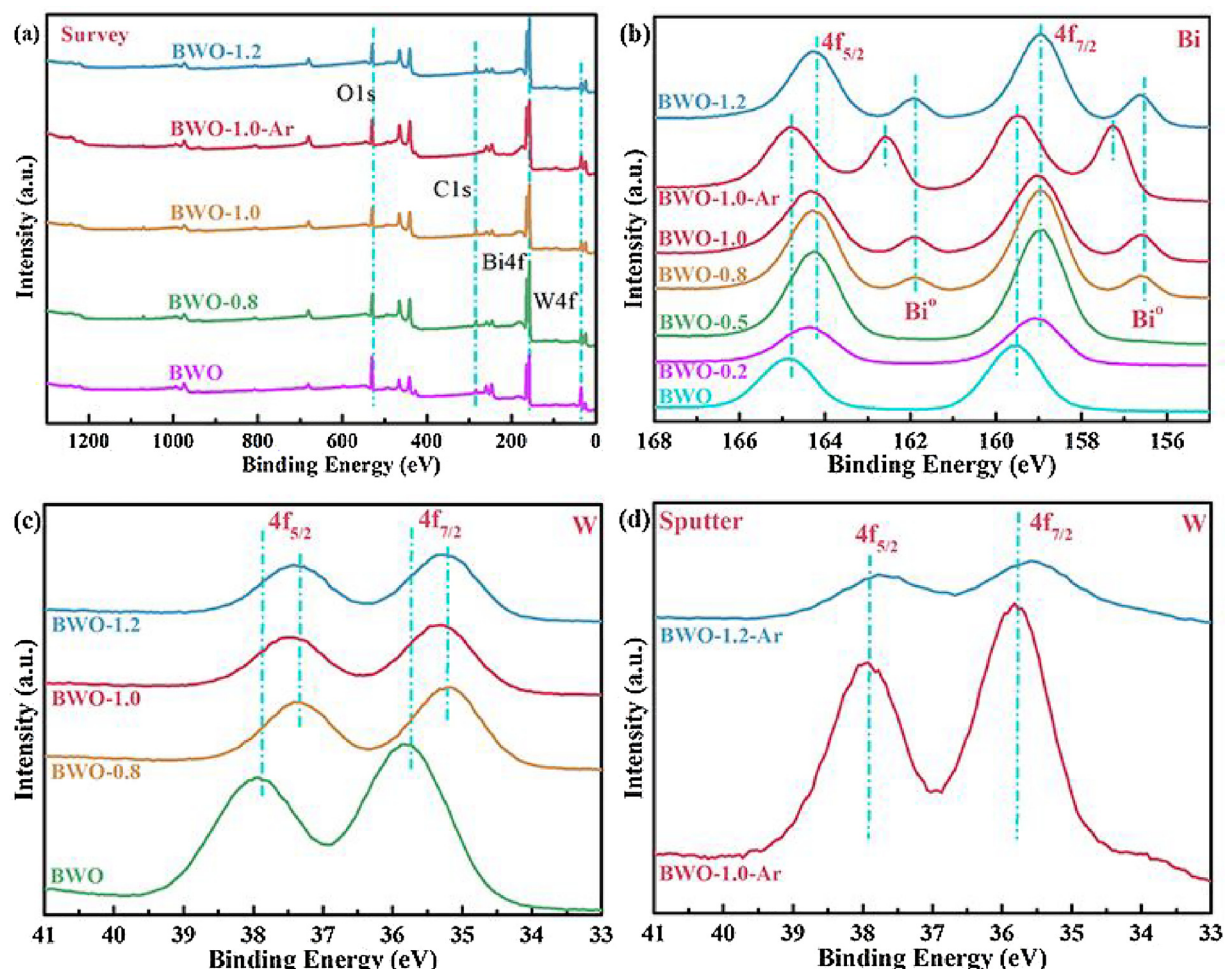


Fig. 3. XPS spectra of Bi–BWO: survey (a), Bi 4f (b), W 4f(c), W 4f sputter (d).

The sample for ESR measurement (FLsp920, U.K.) was prepared by mixing Bi_2WO_6 in a 50 mM DMPO solution with aqueous dispersion for DMPO- $\cdot\text{OH}$ and methanol dispersion for DMPO- $\cdot\text{O}_2^-$. In situ DRIFTS measurements (VERTEX70 FTIR spectrometer, Bruker) equipped with an in situ diffuse-reflectance cell (Harrick) were conducted to understand the related photocatalytic oxidation processes over catalyst.

2.3. Visible light photocatalytic NO removal

The photocatalytic activity was evaluated by the removal efficiency of NO at ppb levels in a continuous flow reactor at ambient temperature. The rectangular reactor (30 cm \times 15 cm \times 10 cm) is made of polymeric glass and covered with Saint-Glass. A commercial tungsten halogen lamp (150 W) was vertically placed outside and 20 cm above the reactor. The UV light in the light beam was removed by adopting a UV cutoff filter (420 nm). The average light intensity is 0.16 W/cm². The as-prepared sample (0.20 g) was dispersed in absolute ethyl alcohol (25 mL) via ultrasonic treatment. The resulting suspension was coated onto two glass dishes (12.00 cm in diameter) and then pretreated at 55 °C to remove ethyl alcohol. The NO gas acquired from a compressed gas cylinder at a concentration of 100 ppm of NO (N₂ balance). The initial concentration of NO was diluted to about 550 ppb by a zero air generator. And the relative humidity (RH) level of the NO flow was controlled at 50% by passing the air stream through a humidification chamber. The flow rates of the air stream and NO were controlled at 2.4 L/min and 15 mL/min, respectively. The lamp was turned on when the adsorption-desorption equilibrium was achieved. The concentration of NO was continuously measured by a NO_x analyzer (Thermo

Environmental Instruments Inc., model 42c-TL), which can monitor the concentration of NO, NO₂ and NO_x (NO_x represents NO + NO₂). The removal ratio (η) of NO was calculated as $\eta = (1 - C/C_0) \times 100\%$, where C and C_0 are the concentrations of NO in the outlet steam and the feeding stream, respectively.

2.4. In situ DRIFT investigation

In situ DRIFTS experiments were carried out by using Bruker Tensor 27 FT-IR spectrometers (Fig. 1). Catalysts were pretreated at room temperature under Helium (30 mL min⁻¹) for 60 min to remove adsorbed impurities. After the background spectrum was recorded with the flowing of Helium and was subtracted, the samples were then exposed to 50 ppm of NO with 20% O₂. DRIFTS spectra of samples were recorded at room temperature by accumulating 32 scans with a resolution of 4 cm⁻¹ at a given interval.

3. Results and discussion

3.1. Catalyst synthesis and formation mechanism

The activation process is achieved through the in situ reduction of Bi_2WO_6 by NaBH₄. In the Bi_2WO_6 system, $(\text{BiO})^+$ and WO_4^{2-} could both react with NaBH₄. Due to the higher redox potential of $\text{WO}_4^{2-}/\text{WO}_3^{2-}$ to that of $(\text{BiO})^+/\text{Bi}^0$, WO_4^{2-} should be reduced prior to $(\text{BiO})^+$. Fig. 2 presents the XRD patterns of the as-synthesized Bi_2WO_6 and BWO-X composites, respectively. The Bi_2WO_6 particle in an amorphous nature is indicated by the only one broad diffraction peak at 29° on its

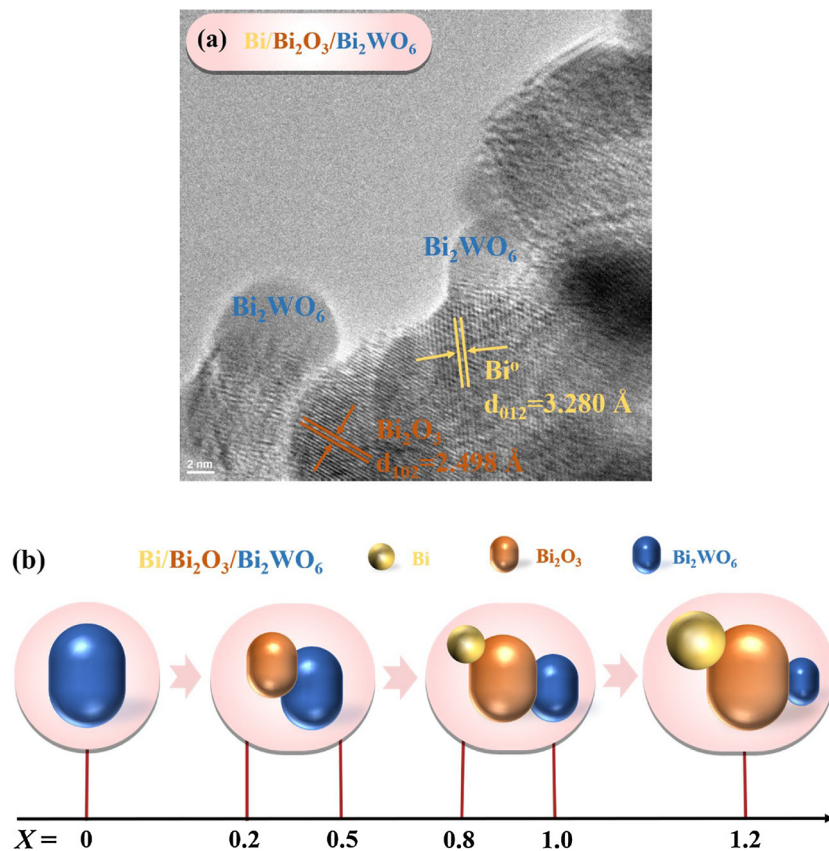


Fig. 4. The HRTEM images of BWO-0.8 (a). The X-dependent phase conversion in the series of BWO samples (b).

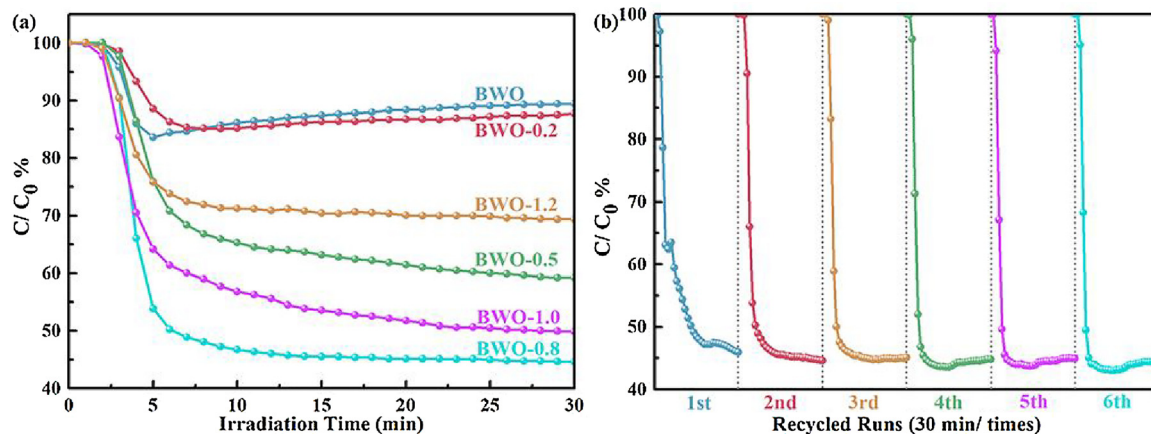


Fig. 5. Visible light photocatalytic activities of pure Bi_2WO_6 and BWO-X ($X = 0.2, 0.5, 0.8, 1.0, 1.2$) for NO removal (a), Cycling runs of BWO-0.8 under visible light irradiation (b).

XRD pattern. After addition of a small amount of NaBH_4 ($\text{NaBH}_4/\text{Bi}_2\text{WO}_6$ molar ratio = 0.2 and 0.5), three new peaks at around 26° , 32° and 34° emerge, which can be all assigned to Bi_2O_3 . With a further addition of NaBH_4 with a molar ratio of $\text{NaBH}_4/\text{Bi}_2\text{WO}_6$ (0.8–1.2), another four diffraction peaks at 27.3° , 28° and 39.8° of metallic Bi phase (JCPDSNo.05-0519) are observed, while the peaks of Bi_2O_3 are weakened and that of Bi_2WO_6 disappears. It is supposed that the initial reduction of WO_4^{2-} will drive the phase conversion of $(\text{BiO})^+$ to Bi_2O_3 , and the generated Bi_2O_3 can be further reduced to metallic Bi phase by the excess NaBH_4 .

To further explore the reaction pathway of Bi_2WO_6 reduction by NaBH_4 , X-ray photoelectron spectroscopy (XPS) analyses were then carried out on all the samples. The XPS survey spectra in Fig. 3a show

the presence of the element Bi , W and O in all the studied BWO composites. All the XPS spectra were calibrated using $\text{C} 1s$ standard peak located at 284.8 eV as a reference. Fig. 3b presents the high-resolution XPS spectra of Bi . In the as-synthesized Bi_2WO_6 , Bi^{3+} is confirmed by the $\text{Bi} 4f_{7/2}$ and $\text{Bi} 4f_{5/2}$ characteristic peaks lying at 164.87 and 159.57 eV, respectively. In BWO-X, both the two $\text{Bi} 4f$ peaks, however, shift to lower binding energies, suggesting that the Bi^{3+} has been partially reduced by NaBH_4 in all the samples. The metallic Bi° is only detectable in BWO-0.8, BWO-1.0 and BWO-1.2, which is consistent with the XRD results. The undetectable metallic Bi° in BWO-0.2 and 0.5 may originate from the oxidation of the small amount of Bi° in BWO-0.2 and 0.4 when exposed to air. The high-resolution XPS spectra of W are also examined, and the results in Fig. 3c show that the $\text{W} 4f_{5/2}$ and W

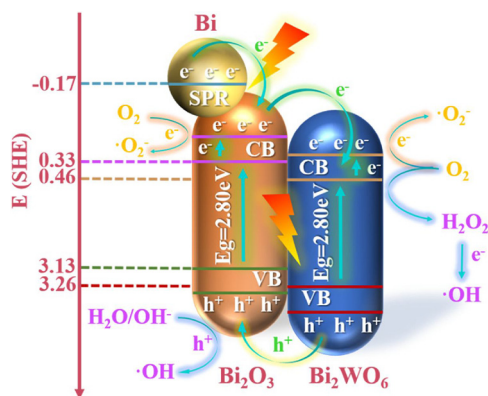
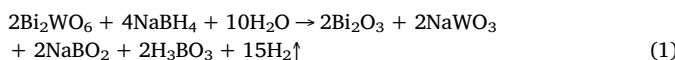


Fig. 6. Schematic diagram of electron-hole pairs separation and the possible reaction mechanism of Bi/Bi₂WO₆/Bi₂O₃ under visible light irradiation.

4f_{7/2} peaks in all BWO-X show a negative shift compared to those in the as-synthesized Bi₂WO₆, indicating that the WO₄²⁻ has been partially reduced. We further sputter away 30 nm-thick surface chemicals on the sample BWO-1.0 and 1.2 (Fig. 3d). It is found that the W 4f_{5/2} and W 4f_{7/2} in the sputtered BWO-X show the same peak position with those of the original Bi₂WO₆, but their peak intensity decreases with the increasing NaBH₄/Bi₂WO₆ molar ratio from 1.0 to 1.2. It means that some Bi₂WO₆ is still retained in the composites.

The morphology and structure change in BWO-X was investigated by SEM and HRTEM. The SEM results in Fig. S1 shows that all the samples appear as irregular embossment, and little difference is actually observed between BWO-X. Fig. 4a presents the HRTEM image of one typical sample BWO-0.8.0.8. It shows the clear lattice fringes with two spacings of 2.498 Å and 3.280 Å, which can be indexed to (102) and (012) crystal planes of Bi₂O₃ and Bi, respectively. The amorphous Bi₂WO₆ can also be differentiated by the part where no lattice fringe can be observed.

The combination of the XRD, XPS and HRTEM results demonstrates that the ternary Bi/Bi₂O₃/Bi₂WO₆ composite could be successfully constructed by a facile reduction of Bi₂WO₆ by NaBH₄, and the by-products were removed after rinsing. Therefore, a two-step reaction pathway is proposed as follows:



Accordingly, the composition of the catalyst depends much on the dosage of NaBH₄, and the X-dependent composition evolution can be schemed in Fig. 4b. With an increased NaBH₄/Bi₂WO₆ ratio, the amount of Bi₂WO₆ decreases, while Bi₂O₃ raises its concentration to the

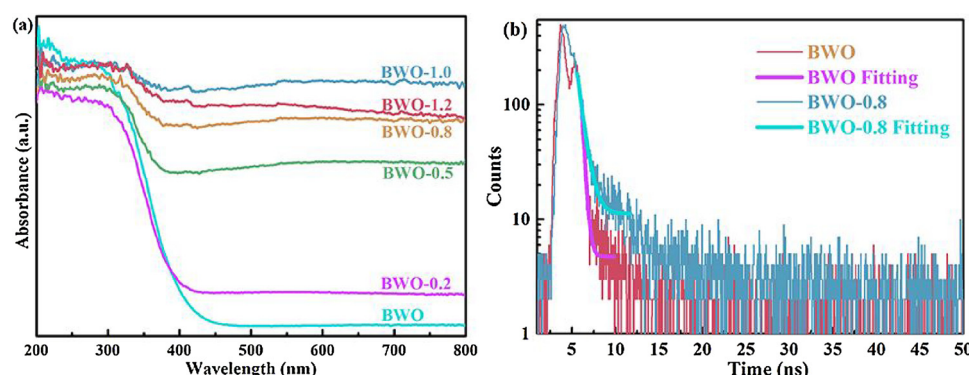


Fig. 7. UV-vis diffuse reflectance spectra of pure amorphous Bi₂WO₆ and BWO-X (X = 0.2, 0.5, 0.8, 1.0, 1.2) (a). The ns-level time-resolved fluorescence spectrum monitored under 400 nm excitation at room temperature for sample Bi₂WO₆ and BWO-0.8 (b).

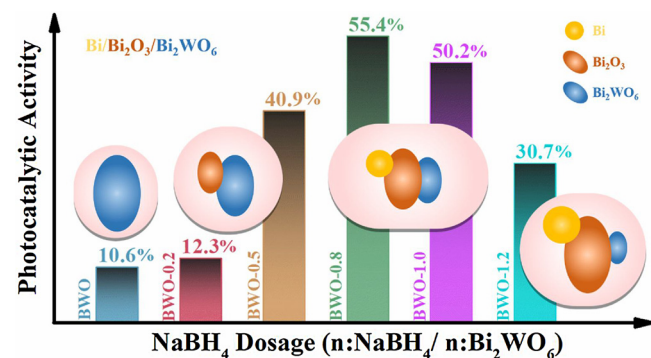


Fig. 8. The relationship between photocatalysis efficiency and substance constituent.

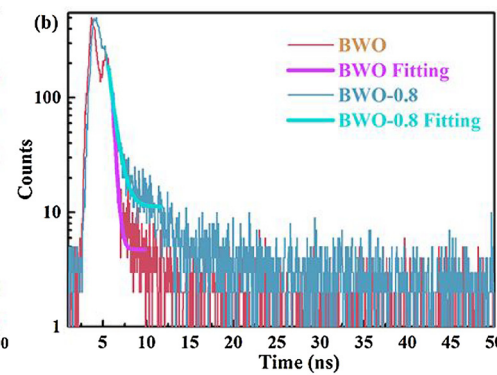
peak at the NaBH₄/Bi₂WO₆ of 0.5, above which more Bi₂O₃ tend to be reduced to Bi.

3.2. Photocatalytic performance

The photocatalytic performance of Bi₂WO₆ and the BWO-X (X = 0.2, 0.5, 0.8, 1.0 and 1.2) for NO removal from a continuous air flow were tested under visible light illumination, and the activity was assessed by the ratio of NO concentration in outlet streams (C) to that in feeding streams (C₀). The results in Fig. 5 show that for all the samples, the NO concentration decreases with the reaction time, but obviously, the BWO-X can remove more amount of NO than Bi₂WO₆, indicating that the deposition of Bi and Bi₂O₃ could indeed activate the inert amorphous Bi₂WO₆. Furthermore, the BWO-X shows an X-dependent photocatalytic activity. With the X increasing from 0.2 to 1.2, the C/C₀ at 30 min decrease from 87.7 to 44.6, reach the lowest of at X = 0.8, and then increases to 69.3. Meanwhile, an ideal photocatalyst also should possess photochemical stability and durability. Fig. 5b shows the result of circulating runs of BWO-0.8, which indicates that the sample is stable during the photocatalytic process.

3.3. Photocatalysis mechanism

In our system, BWO-X comprises the Bi°, Bi₂O₃ and Bi₂WO₆. Bi₂O₃ and Bi₂WO₆ are well-known semiconductor photocatalysts with visible-light-response band gap of 2.80 eV [38] and 2.80 eV [39], respectively, while Bi NP is a plasmonic metal [40]. Under visible light illumination, e⁻/h⁺ pairs are excited and dissociated over the surface of Bi NPs as well as in both the Bi₂O₃ and Bi₂WO₆ semiconductors, leading to a much increased charge carrier concentration. Due to the energy difference in conduction and valance band edge of the two semiconductors as well as the Fermi level of Bi NPs, the three components could form



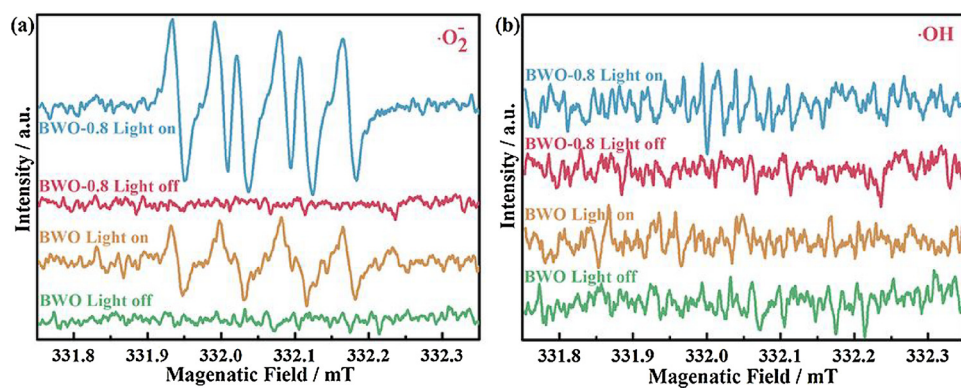


Fig. 9. DMPO spin-trapping ESR spectra of pure amorphous Bi_2WO_6 and BWO-0.8 methanol dispersion for DMPO - $\cdot\text{O}_2^-$ (a) and aqueous dispersion for DMPO - $\cdot\text{OH}$ (b).

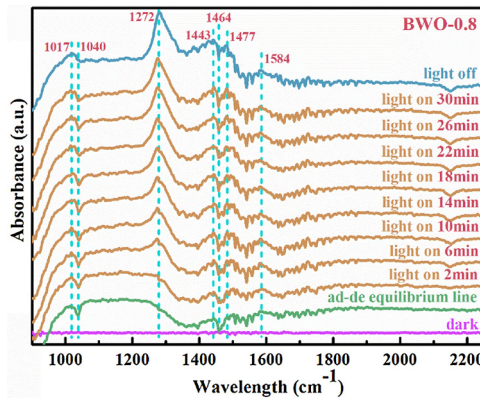


Fig. 10. In situ IR spectra of photocatalytic reaction of NO over BWO-0.8 under ultraviolet light irradiation.

Table 1

Assignments of the IR bands observed during photocatalytic NO oxidation processes over the $\text{Bi}/\text{Bi}_2\text{O}_3/\text{Bi}_2\text{WO}_6$ under visible light irradiation.

Wavenumbers (cm^{-1})	Assignment	References
1017	NO	[43]
1040	NO	[44]
1272	Unidentate nitrate	[45]
1443	NO_2	[46]
1464	NO_2	[46]
1477	Unidentate carbonate	[47]
1584	Bidentate carbonate	[47]

perfect heterojunction structures. Their synergistic interaction could be schemed in Fig. 6. Because of the intimate contact of Bi, Bi_2O_3 and Bi_2WO_6 , and the higher Fermi level of Bi NPs (-0.17 eV) [41] over the conduction band edge of Bi_2O_3 (0.33 eV) and Bi_2WO_6 (0.46 eV), two interfacial heterojunctions, i.e. $\text{Bi}/\text{Bi}_2\text{O}_3$ and $\text{Bi}_2\text{O}_3/\text{Bi}_2\text{WO}_6$, will thus be constructed. It should be noted the heterojunction between Bi and Bi_2WO_6 will not form since the Bi is actually converted from Bi_2O_3 . Accordingly, the excited e^- will spontaneously flow through the heterojunction from Bi to Bi_2O_3 and then to Bi_2WO_6 . Unlike e^- , the separated h^+ directly migrates from Bi_2WO_6 to the surface of Bi_2O_3 to initialize the oxidation reaction. Obviously, such dual heterojunctions can prevent e^-/h^+ recombination in both Bi_2O_3 and Bi_2WO_6 . As a plasmonic metal, Bi NPs will concentrate incident photon energy into plasmon oscillations. Besides the hot electrons, the concentrated resonance energy can be also converted to a local electromagnetic field [32], facilitating the e^-/h^+ separation in $\text{Bi}_2\text{O}_3/\text{Bi}_2\text{WO}_6$. Accordingly, we can conclude that the in situ deposition of Bi and Bi_2O_3 can contribute to an enhanced photocatalysis by increasing the charge carrier

concentration and promoting e^-/h^+ separation via the heterojunction effect and SPR effect.

To prove the formation of heterojunction and the SPR of Bi NPs and their effect on charge carrier concentration, UV-vis diffuse reflectance spectra (DRS) of the pure Bi_2WO_6 and BWO-X ($X = 0.2, 0.5, 0.8, 1.0, 1.2$) were firstly examined, and the results are presented in Fig. 7a. Compared to the pure Bi_2WO_6 , all the BWO-X show an enhanced photo-absorption, indicating the charge carrier is increased in the ternary composite. Considering the substance composition evolution with X (See Fig. 4), the increased photo-absorption in BWO-0.2 and BWO-0.5 should arise from the formation of $\text{Bi}_2\text{O}_3/\text{Bi}_2\text{WO}_6$ heterojunction, while that in BWO-0.8 and BWO-1.0 is more likely to be caused by the synergy effect of the Bi SPR effect and the dual heterojunctions (i.e. $\text{Bi}/\text{Bi}_2\text{O}_3$ and $\text{Bi}_2\text{O}_3/\text{Bi}_2\text{WO}_6$). The reason why the photo-absorption curve of BWO-1.2 is lower than BWO-1.0 could be explained by the reduced amount of Bi_2WO_6 in BWO-1.2. The heterojunction and SPR effects on e^-/h^+ separation efficiency were confirmed by the ns-level time-resolved fluorescence decay spectra in sample Bi_2WO_6 and BWO-0.8 (See Fig. 7b). The lifetime of charge carriers is shown to be 0.7003 ns in BWO-0.8, which is much longer than that of 0.3007 ns for BWO.

As demonstrated, the molar ratio of Bi, Bi_2O_3 and Bi_2WO_6 in composite can be modulated by the dosage of NaBH_4 . As a result, the amount of each heterojunction (i.e. $\text{Bi}/\text{Bi}_2\text{O}_3$ or $\text{Bi}_2\text{O}_3/\text{Bi}_2\text{WO}_6$) as well as the intensity of SPR effect could be controlled, and their contribution to photocatalytic performance can be optimized. Fig. 8 shows that the photocatalytic NO removal efficiency ($(1 - C/C_0) \times 100\%$) of BWO-X presents a volcano-like variation with the X. BWO-0.2 sample shows a low activity due to the slight metallic Bi_2O_3 loading. The removal efficiency of NO over BWO-0.8 for 30 min is raised to 55.4%, which can be ascribed to the surface plasmon resonance (SPR) effect of Bi and the Bi_2O_3 forms a heterojunction on Bi_2WO_6 . These SPR and heterojunction effect could improve the separation efficiency of photoexcited charge carriers. And then with much too reduction agent, the activity of BWO-1.2 is decline to 30.7% for the reason that the heterojunction structure of the catalyst is destroyed and lack of Bi_2WO_6 . The result shows that a suitable substance constituent can increase the photocatalysis efficiency, otherwise over reduction is harm to the photocatalyst. According to the result of nitric oxide removal efficiency and XPS analysis, this research reveals the relationship between photocatalysis activity and substance constituent (Fig. 8).

3.4. Photocatalytic reaction pathway of NO oxidation

DMPO-ESR analyses were conducted on pure amorphous Bi_2WO_6 and BWO-0.8 to identify the active radicals and then explore more on the role of Bi NPs and Bi_2O_3 , and the results are presented in Fig. 9. No signals could be observed when the system kept in dark. Under visible light illumination, comparing pure amorphous Bi_2WO_6 and BWO-0.8,

the six characteristic peaks of the DMPO- $\cdot\text{O}_2^-$ adduct can be clearly observed in Fig. 9a, which demonstrates the $\cdot\text{O}_2^-$ has been generated via the reduction of O_2 . And the intensity of the $\cdot\text{O}_2^-$ signal absolutely increased with prolonging the illumination time. The signals from BWO-0.8 are much stronger than that of BWO, which can be ascribed to the more efficient charge separation and transfer. However, the signals of the $\cdot\text{OH}$ can hardly be detected in Fig. 9b after irradiation and the intensity are significantly weaker than $\cdot\text{O}_2^-$ signal. It means that the h^+ participated in the direct oxidation reaction.

In a ternary system of $\text{Bi}/\text{Bi}_2\text{O}_3/\text{Bi}_2\text{WO}_6$, the energy of the photo-excited e^- and h^+ depends mainly on the band-edge position of the conduction band of Bi_2WO_6 and valence band of Bi_2O_3 , lying theoretically at 0.46 and 3.26 eV, respectively. Upon such a positive conduction band-edge potential, oxygen molecule (O_2) in air was reduced into oxidative $\cdot\text{O}_2^-$ radical by the e^- transfer from bottom to top of conduction band of Bi_2O_3 and Bi_2WO_6 (Note that the conduction band has a certain breadth, so electrons can be photoexcited to higher levels of conduction bands) [42], instead of the e^- from conduction band bottom of Bi_2O_3 or Bi_2WO_6 as the redox potential for O_2 into $\cdot\text{O}_2^-$ is -0.33 eV, and not support the conversion for NO to N_2 (the redox potential is -1.67 eV). The electrons gathering at the conduction band of Bi_2WO_6 can reduce O_2 to H_2O_2 as the redox potential of O_2 into H_2O_2 is 0.695 eV and the formed H_2O_2 would be further transformed into $\cdot\text{OH}$ by capturing an electron. The h^+ with the potential of 3.26 eV can trigger the $\cdot\text{OH}$ oxidative radical via $\text{h}^+ + \text{H}_2\text{O} \rightarrow \cdot\text{OH} + \text{H}^+$ (1.99 eV), and the h^+ also can directly oxidize NO. Accordingly, the oxidative radicals $\cdot\text{O}_2^-$, $\cdot\text{OH}$, h^+ are the potential agents for removing NO at ppb level.

In situ DRIFTS studies were further performed to understand the related photocatalytic NO oxidation processes over the $\text{Bi}/\text{Bi}_2\text{O}_3/\text{Bi}_2\text{WO}_6$. Fig. 10 shows the time evolution of the IR spectra under visible light irradiation. And this process keeps a steady-state condition that the concentration of NO is 50 ppm and the gas flow rate is 25 mL/min. The ad-de equilibrium line that represents the equilibrium state of NO adsorption process was used for a reference to clearly observe the transformation between reaction intermediate products in photocatalytic processes. A broad absorption peaks from 1000 cm^{-1} to 1300 cm^{-1} showed in ad-de equilibrium line can be ascribed to the $\text{NO} + \text{O}_2$ adsorption process. The generated band at 1017 cm^{-1} and the consumed band at 1040 cm^{-1} caused by vibration and rotation of NO , meanwhile, the generated band at 1443 cm^{-1} and the consumed band at 1464 cm^{-1} caused by vibration and rotation of NO_2 can be observed, indicated that the partial of adsorbed NO has been oxidized into NO_2 and then converts into other intermediate products after irradiation. With the irradiation of visible light, the generated peak at 1272 cm^{-1} and the intensity increased gradually over time assigned to unidentate nitrates have been detected which is consistent with previous analysis that NO_2 has been changed into unidentate nitrates caused by the oxidative radicals generated from $\text{Bi}/\text{Bi}_2\text{O}_3/\text{Bi}_2\text{WO}_6$. The final products could be removed easily by water washing and the photocatalyst can be regenerated via this facile method. In summary, the main observed IR bands of the adsorbed species and their chemical assignments are listed in supporting information (Table 1). The transformation of reaction product demonstrated the photocatalytic oxidation processes for NO removal directly and also further explain the efficient photocatalytic activity of the $\text{Bi}/\text{Bi}_2\text{O}_3/\text{Bi}_2\text{WO}_6$.

4. Conclusion

In summary, the non-noble metal Bi and Bi_2O_3 were produced from amorphous Bi_2WO_6 via an in situ reduction method with NaBH_4 as the reducing agent. The molar ratio of Bi, Bi_2O_3 and Bi_2WO_6 in composite can be modulated by the dosage of NaBH_4 , and consequently the amount of each heterojunction (i.e. $\text{Bi}/\text{Bi}_2\text{O}_3$ or $\text{Bi}_2\text{O}_3/\text{Bi}_2\text{WO}_6$) as well as the intensity of SPR effect could be controlled. Then the ternary system of $\text{Bi}/\text{Bi}_2\text{O}_3/\text{Bi}_2\text{WO}_6$ photocatalyst was constructed. Compared

with pure amorphous Bi_2WO_6 , the Bi-loaded Bi_2WO_6 and the $\text{Bi}_2\text{O}_3/\text{Bi}_2\text{WO}_6$ structure, the ternary system of $\text{Bi}/\text{Bi}_2\text{O}_3/\text{Bi}_2\text{WO}_6$ photocatalyst possessed better visible light absorption, higher charge separation rate because of the synergistic effect of heterojunction and SPR, enabling the system exhibited the high electron transfer ability. Based on these merits, the Bi and Bi_2O_3 loaded ternary photocatalyst performs highly enhanced photocatalytic activity for the NO removal under visible light irradiation. This work may shed new light on the development of polybasic materials synthesis and activate amorphous semiconductor photocatalyst for environmental applications.

Acknowledgements

This work was supported by the National Natural Science Foundation of China (21501016, 21777011 and 51478070), the National Key R&D Plan (2016YFC02047), the Innovative Research Team of Chongqing (CXTDG201602014), the Key Natural Science Foundation of Chongqing (cstc2017jcyjBX0052) and Innovation Research Project of Postgraduate from CTBU (yjcx2017-066-64), Chongqing Postdoctoral Science Foundation Funded Project (Xm2016020), Natural Science Foundation of Chongqing Science & Technology Commission (cstc2016jcyjA0154). The authors also acknowledge the AM-HPC in Suzhou, China for computational support.

Appendix A. Supplementary data

Supplementary material related to this article can be found, in the online version, at doi:<https://doi.org/10.1016/j.apcatb.2018.03.047>.

References

- [1] X. Li, J. Yu, J. Low, Y. Fang, J. Xiao, X. Chen, Engineering heterogeneous semiconductors for solar water splitting, *J. Mater. Chem. A* 3 (2015) 2485–2534.
- [2] H. Huang, Y. He, X. Li, M. Li, C. Zeng, F. Dong, X. Du, T. Zhang, Y. Zhang, $\text{Bi}_2\text{O}_2(\text{OH})(\text{NO}_3)$ as a desirable $[\text{Bi}_2\text{O}_2]^{2+}$ layered photocatalyst: strong intrinsic polarity, rational band structure and {001} active facets co-beneficial for robust photooxidation, *J. Mater. Chem. A* 3 (2015) 24547–24556.
- [3] C. Wang, X. Zhang, Y. Liu, Promotion of multi-electron transfer for enhanced photocatalysis: a review focused on oxygen reduction reaction, *Appl. Surf. Sci.* 358 (2015) 28–45.
- [4] X. Wang, K. Maeda, A. Thomas, K. Takanabe, G. Xin, J.M. Carlsson, K. Domen, M. Antonietti, A metal-free polymeric photocatalyst for hydrogen production from water under visible light, *Nat. Mater.* 8 (2009) 76–80.
- [5] H. Wang, W. Zhang, X. Li, J. Li, W. Cen, Q. Li, F. Dong, Highly enhanced visible light photocatalysis and in situ FT-IR studies on Bi metal@defective BiOCl hierarchical microspheres, *Appl. Catal. B Environ.* 225 (2018) 218–227.
- [6] Y. Huang, Y. Liang, Y. Rao, D. Zhu, J. Cao, Z. Shen, W. Ho, S. Lee, Environment-friendly carbon quantum dots/ ZnFe_2O_4 photocatalysts: characterization, biocompatibility and mechanisms for NO removal, *Environ. Sci. Technol.* 51 (2017) 2924–2933.
- [7] C. Pan, J. Xu, Y. Wang, D. Li, Y. Zhu, Dramatic activity of $\text{C}_3\text{N}_4/\text{BiPO}_4$ photocatalyst with core/shell structure formed by self-assembly, *Adv. Funct. Mater.* 22 (2012) 1518–1524.
- [8] Z. Wang, Y. Huang, W. Ho, J. Cao, Z. Shen, S. Lee, Fabrication of $\text{Bi}_2\text{O}_2\text{CO}_3/\text{g-C}_3\text{N}_4$ heterojunctions for efficiently photocatalytic NO in air removal: in-situ self-sacrificial synthesis, *Charact. Mech. Study Appl. Catal. B Environ.* 199 (2016) 123–133.
- [9] W. Cui, J. Li, F. Dong, Y. Sun, G. Jiang, W. Cen, S.C. Lee, Z. Wu, Highly efficient performance and conversion pathway of photocatalytic NO oxidation on SrO -clusters@amorphous carbon nitride, *Environ. Sci. Technol.* 51 (2017) 10682–10690.
- [10] J. Bi, L. Wu, J. Li, Z. Li, X. Wang, X. Fu, Simple solvothermal routes to synthesize nanocrystalline Bi_2MoO_6 photocatalysts with different morphologies, *Acta Mater.* 55 (2007) 4699–4705.
- [11] K. Jing, J. Xiong, N. Qin, Y. Song, L. Li, Y. Yu, S. Liang, L. Wu, Development and photocatalytic mechanism of monolayer Bi_2MoO_6 nanosheets for the selective oxidation of benzylic alcohols, *Chem. Commun.* 53 (2017) 8604–8607.
- [12] H. Huang, S. Tu, C. Zeng, T. Zhang, A.H. Reshak, Y. Zhang, Macroscopic polarization enhancement promoting photo- and piezoelectric-induced charge separation and molecular oxygen activation, *Angew. Chem.-Int. Ed.* 56 (2017) 11860–11864.
- [13] H. Huang, K. Xiao, Y. He, T. Zhang, F. Dong, X. Du, Y. Zhang, In situ assembly of $\text{BiO}@\text{Bi}_2\text{O}_1\text{Cl}_2\text{p-n}$ junction: charge induced unique front-lateral surfaces coupling heterostructure with high exposure of BiO {001} active facets for robust and nonselective photocatalysis, *Appl. Catal. B Environ.* 199 (2016) 75–86.
- [14] H. Huang, R. Cao, S. Yu, X. Xu, W. Hao, Y. Wang, F. Dong, T. Zhang, Y. Zhang, Single-unit-cell layer established Bi_2WO_6 3D hierarchical architectures: efficient adsorption, photocatalysis and dye-sensitized photoelectrochemical performance, *Appl. Catal. B Environ.* 219 (2017) 526–537.

[15] H. Fu, L. Zhang, W. Yao, Y. Zhu, Photocatalytic properties of nanosized Bi_2WO_6 catalysts synthesized via a hydrothermal process, *Appl. Catal. B: Environ.* 66 (2006) 100–110.

[16] L. Wu, J. Bi, Z. Li, X. Wang, X. Fu, Rapid preparation of Bi_2WO_6 photocatalyst with nanosheet morphology via microwave-assisted solvothermal synthesis, *Catal. Today* 131 (2008) 15–20.

[17] H. Fu, C. Pan, W. Yao, Y. Zhu, Visible-light-induced degradation of rhodamine b by nanosized Bi_2WO_6 , *J. Phys. Chem. B* 109 (2005) 22432–22439.

[18] J. Yu, J. Xiong, B. Cheng, Y. Yu, J. Wang, Hydrothermal preparation and visible-light photocatalytic activity of Bi_2WO_6 powders, *J. Solid State Chem.* 178 (2005) 1968–1972.

[19] W.T. Liu, S. Cochrane, S.T. Lakshmikumar, D.B. Knorr, E.J. Rymaszewski, J.M. Borrego, T.M. Lu, Low-temperature fabrication of amorphous $\text{BaTiO}_3/\text{sub 3/}$ Thin-film bypass capacitors, *IEEE Electron. Device Lett.* 14 (1993) 320–322.

[20] Y. Si, G. Liu, C. Deng, W. Liu, H. Li, L. Tang, Facile synthesis and electrochemical properties of amorphous FeVO_4 as cathode materials for lithium secondary batteries, *J. Electroanal. Chem.* 787 (2017) 19–23.

[21] S. Narushima, H. Mizoguchi, K.I. Shimizu, K. Ueda, H. Ohta, M. Hirano, T. Kamiya, H. Hosono, A p-type amorphous oxide semiconductor and room temperature fabrication of amorphous oxide p-n heterojunction diodes, *Adv. Mater.* 15 (2003) 1409–1413.

[22] K. Nomura, H. Ohta, A. Takagi, T. Kamiya, M. Hirano, H. Hosono, Room-temperature fabrication of transparent flexible thin-film transistors using amorphous oxide semiconductors, *Nature* 432 (2004) 488–492.

[23] V.A. Lebedev, D.A. Kozlov, I.V. Kolesnik, A.S. Poluboyarinov, A.E. Becerikli, W. Grünert, A.V. Garshev, The amorphous phase in titania and its influence on photocatalytic properties, *Appl. Catal. B: Environ.* 195 (2016) 39–47.

[24] Y. Kim, H.M. Hwang, L. Wang, I. Kim, Y. Yoon, H. Lee, Solar-light photocatalytic disinfection using crystalline/amorphous low energy bandgap reduced TiO_2 , *Sci. Rep.* 6 (2016) 2–11.

[25] Fridman, Review of the theory of amorphous semiconductors, *J. Non Cryst. Solids* 4 (1970) 391–409.

[26] J. Yan, G. Wu, N. Guan, L. Li, Z. Li, X. Cao, Understanding the effect of surface/bulk defects on the photocatalytic activity of TiO_2 : anatase versus rutile, *Phys. Chem. Chem. Phys.* 15 (2013) 10978–10988.

[27] A. Kudo, K. Omori, H. Kato, A novel aqueous process for preparation of crystal form-controlled and highly crystalline BiVO_4 powder from layered vanadates at room temperature and its photocatalytic and photophysical properties, *J. Am. Chem. Soc.* 121 (1999) 11459–11467.

[28] M. Kong, Y. Li, X. Chen, T. Tian, P. Fang, F. Zheng, X. Zhao, Tuning the relative concentration ratio of bulk defects to surface defects in TiO_2 nanocrystals leads to high photocatalytic efficiency, *J. Am. Chem. Soc.* 133 (2011) 16414–16417.

[29] X. Zhang, J. Qin, Y. Xue, P. Yu, B. Zhang, L. Wang, R. Liu, Effect of aspect ratio and surface defects on the photocatalytic activity of ZnO nanorods, *Sci. Rep.* 4 (2014) 4–11.

[30] F. Amano, A. Yamakata, K. Nogami, M. Osawa, B. Ohtani, Visible light responsive pristine metal oxide photocatalyst: enhancement of activity by crystallization under hydrothermal treatment, *J. Am. Chem. Soc.* 130 (2008) 17650–17651.

[31] X. Li, Y. Sun, T. Xiong, G. Jiang, Y. Zhang, Z. Wu, F. Dong, Activation of amorphous bismuth oxide via plasmonic Bi metal for efficient visible-light photocatalysis, *J. Catal.* 352 (2017) 102–112.

[32] T. Xiong, X. Dong, H. Huang, W. Cen, Y. Zhang, F. Dong, Single precursor mediated-synthesis of bi semimetal deposited N-doped $(\text{BiO})_2\text{CO}_3$ superstructures for highly promoted photocatalysis, *ACS Sustain. Chem. Eng.* 4 (2016) 2969–2979.

[33] Y. Yu, C. Cao, H. Liu, P. Li, F. Wei, Y. Jiang, W. Song, A Bi/BiOCl heterojunction photocatalyst with enhanced electron–hole separation and excellent visible light photodegrading activity, *J. Mater. Chem. A* 2 (2014) 1677–1681.

[34] Z. Zhao, W. Zhang, Y. Sun, J. Yu, Y. Zhang, H. Wang, F. Dong, Z. Wu, Bi cocatalyst/ Bi_2MoO_6 microspheres nanohybrid with SPR-promoted visible-light photocatalysis, *J. Phys. Chem. C* 120 (2016) 11889–11898.

[35] F. Dong, Z. Zhao, Y. Sun, Y. Zhang, S. Yan, Z. Wu, An advanced semimetal-organic Bi spheres/g-C₃N₄ nanohybrid with SPR-enhanced visible-light photocatalytic performance for NO purification an advanced semimetal-organic bi spheres/g-C₃N₄ nanohybrid with SPR-enhanced visible-light photocatalytic per, *Environ. Sci. Technol.* 49 (2015) 12432–12440.

[36] G. Jiang, X. Li, M. Lan, T. Shen, X. Lv, F. Dong, S. Zhang, Monodisperse bismuth nanoparticles decorated graphitic carbon nitride: enhanced visible-light-response photocatalytic NO removal and reaction pathway, *Appl. Catal. B: Environ.* 205 (2017) 532–540.

[37] S. Verma, B.T. Rao, S. Bhartiya, V. Sathe, L.M. Kukreja, Growth temperature dependent surface plasmon resonances of densely packed gold nanoparticles' films and their role in surface enhanced Raman scattering of Rhodamine6G, *Appl. Surf. Sci.* 346 (2015) 379–387.

[38] Z. Bian, J. Zhu, S. Wang, Y. Cao, X. Qian, H. Li, Self-assembly of active $\text{Bi}_2\text{O}_3/\text{TiO}_2$ visible photocatalyst with ordered mesoporous structure and highly crystallized anatase, *J. Phys. Chem. C* 112 (2008) 6258–6262.

[39] Q.C. Xu, D.V. Wellia, Y.H. Ng, R. Amal, T.T.Y. Tan, Synthesis of porous and visible-light absorbing $\text{Bi}_2\text{WO}_6/\text{TiO}_2$ heterojunction films with improved photoelectrochemical and photocatalytic performances, *J. Phys. Chem. C* 115 (2011) 7419–7428.

[40] F. Dong, T. Xiong, Y. Sun, H. Huang, Z. Wu, Synergistic integration of thermocatalysis and photocatalysis on black defective $(\text{BiO})_2\text{CO}_3$ microspheres, *J. Mater. Chem. A* 3 (2015) 18466–18474.

[41] S. Yu, H. Huang, F. Dong, M. Li, N. Tian, T. Zhang, Y. Zhang, Synchronously achieving plasmonic bi metal deposition and I-doping by utilizing BiOIO_3 as the self-sacrificing template for high-performance multifunctional applications, *ACS Appl. Mater. Interfaces* 7 (2015) 27925–27933.

[42] X. Dong, W. Zhang, Y. Sun, J. Li, W. Cen, Z. Cui, H. Huang, F. Dong, Visible-light-induced charge transfer pathway and photocatalysis mechanism on Bi semimetal@defective BiOBr hierarchical microspheres, *J. Catal.* 357 (2018) 41–50.

[43] K.I. Hadjiivanov, Identification of neutral and charged NxOy surface species by IR spectroscopy, *Catal. Rev. Sci. Eng.* 42 (2000) 71–144.

[44] D. Pozdnyakov, V. Filimonov, K. Katal, Infrared spectroscopic study of the chemisorption of nitric oxide and nitrogen dioxide on metal oxides, *Kinet. Catal.* 14 (1973) 760–766.

[45] K. Hadjiivanov, V. Avreyska, D. Klissurski, T. Marinova, Surface species formed after NO adsorption and $\text{NO} + \text{O}_2$ coadsorption on ZrO_2 and sulfated ZrO_2 : an FTIR spectroscopic study, *Langmuir* 18 (2002) 1619–1625.

[46] S.-J. Huang, A.B. Walters, M.A. Vannice, Adsorption and decomposition of NO on lanthanum oxide, *J. Catal.* 192 (2000) 29–47.

[47] G. Ramis, G. Busca, V. Lorenzelli, P. Forzatti, Fourier transform-infrared study of the adsorption and coadsorption of nitric oxide, nitrogen dioxide and ammonia on and mechanism of selective catalytic reduction, *Appl. Catal.* 64 (1990) 243–257.